CRYSTAL GROWTH & DESIGN

Article

Molecular Association Induced Emission Shifts for E/Z Isomers and Selective Sensing of Nitroaromatic Explosives

Matthew J Hurlock, Yuwei Kan, Thibaut Lécrivain, Joseph Lapka, Kenneth L. Nash, and Qiang Zhang

Cryst. Growth Des., **Just Accepted Manuscript** • DOI: 10.1021/acs.cgd.8b01065 • Publication Date (Web): 31 Aug 2018

ACS Publications

is published by the American Chemical Society. 1155 Sixteenth Street N.W., Washington, DC 20036

Molecular Association Induced Emission Shifts for *E*/*Z* Isomers and Selective Sensing of Nitroaromatic Explosives

Matthew J. Hurlock,[†] Yuwei Kan,[‡] Thibaut Lécrivain,[†] Joseph Lapka,[†] Kenneth L. Nash[†], and Qiang Zhang*[, †, §]

[†]Department of Chemistry, [§]Materials Science and Engineering Program, Washington State University, Pullman, WA 99164, USA.

[‡]Department of Chemistry, University of Idaho, Moscow, ID 83844, USA

ABSTRACT: Two 1,2-disubstituted tetraphenylethylene *E*/*Z* isomers, each containing two cyano-functional groups, were successfully synthesized and characterized. Unlike conventional tetraphenylethylene molecules, the two isomers possess unique aggregation induced emission red-shift and enhancement behavior. Interestingly, the crystalline solids of these two isomers show distinct emission maxima which are more than 50 nm apart from each other. These two isomers can selectively detect nitroaromatics, showing a quenching efficiency of picric acid more than 100 times higher than other nitroaromatics. The structural characterization, absorption, and emission in solutions as well as DFT calculations were conducted to help us gain deep insights into the chemistry of these species.

INTRODUCTION

Luminescent molecules and materials have been extensively studied in the past thanks to their tunable emission colors and applications in sensing, imaging, and lighting.[1-8] Of these, systems that exhibit aggregation induced emission (AIE) or aggregation induced emission enhancement (AIEE) characteristics have attracted considerable attention owing to the highly emissive nature of their solids.[9] The AIE behaviour of TPE molecules is attributed to restricted intramolecular rotations (RIR).[10] In contrast with aggregation-caused quenching (ACQ), molecules of the AIE type are promising candidates for fabricating devices, often used as solid powders or crystals.[9] Tetraphenylethene (TPE) based molecules have been comprehensively studied for imaging, sensing, and lighting because of their high quantum efficiency, low-cost, and high tunablility.[9, 11-13] TPE struts have also been used to build organic light-emitting diodes (OLEDs),[14] fluorometric probes,[15-16] luminescent MOFs[7, 17-24] and HOFs[25] for lighting and detection applications.

Throughout the literature, highly symmetric tetra-*para*-substituted TPE molecules have been used to construct MOFs or organic polymers.[18, 26-28] This is because the starting materials are commercially available, and the desired products are easy to synthesize and separate. Di-substituted TPE molecules are often used as *E*/*Z* mixtures,[29-30] as the separation of isomers is difficult. Few studies have focused on the isomerization of TPE molecules. *E*/*Z* isomerization takes place under UV irradiation for some molecules,[31] while it is not observed in other cases.[32] Nevertheless, the *E*/*Z* isomers of TPE molecules behave differently in solution and upon aggregation when interacting with substrates.[33] Thus, it is important to study these *E*/*Z* isomers to help us gain deep insights into the working mechanisms for the design of new molecules and materials for a variety of applications.

Herein, we report the synthesis and

characterization of two dicyano-substituted TPE isomers, (*E*)-4,4'-(1,2-diphenylethene-1,2-diyl)dibenzonitrile, ***E*-1**, and (*Z*)-4,4'-(1,2-diphenylethene-1,2-diyl)dibenzonitrile, ***Z*-1**. Different from conventional AIE molecules, ***E*-1** and ***Z*-1** possess not only aggregation induced emission enhancement, but also aggregation induced emission red-shift behavior. More interestingly, the crystalline solids of ***E*-1** and ***Z*-1** show very distinct emissions upon excitation at the same wavelength. Photoluminescent spectra as well as DFT calculations of both molecules were investigated to help us understand the differences between the two isomers.

EXPERIMENTAL SECTION

Materials. 4-Bromobenzophenone and titanium tetrachloride were purchased from Alfa Aesar. Copper(I) cyanide was purchased from Strem Chemicals. Zinc powder was purchased from VWR International. All chemicals were used as received without further purification. Tetrahydrofuran (THF) was dried by distillation over sodium under nitrogen. N,N-dimethylformamide (DMF) and Acetonitrile were dried using a Vigor Solvent Purification System under nitrogen prior to use. 1,2-bis(4-bromophenyl)-1,2-diphenylethene ($TPEBr_2$) was synthesized following a previously reported procedure.[34]

Instrumentation. UV-Vis spectra were measured on a Thermo Scientific Evolution 300 UV/Vis spectrophotometer. FTIR spectra were obtained on a Thermo Scientific Nicolet™ iS™ 10 spectrometer. ^{1}H and ^{13}C NMR spectra were obtained using a Varian 400-MR NMR spectrometer. Photoluminescent spectra and sensing experiments were obtained with a Horiba FluoroMax-4 fluorometer equipped with a Xeon lamp. Luminescent lifetime measurements were obtained using a Horiba Fluorolog with PMT detector and using a NanoLED 270 excitation source and FluoroHub-B pulse controller. Crystallographic data were obtained using a Bruker SMART Fixed Chi Mo X-Ray source small molecule diffractometer with APEX II CCD detector. MS spectra were measured on a Waters Q-Tof Premier Quadrupole-Time of Flight Mass Spectrometer.

Synthesis of 4,4'-(1,2-diphenylethene-1,2-diyl)dibenzonitrile ($TPE(CN)_2$): Modifications were made to a previously published procedure.[27] $TPEBr_2$ (0.848 g, 1.73 mmol) and CuCN (1.048 g, 11.69 mmol) were added to a 250 mL round-bottom flask with a reflux water condenser. The flask was evacuated by vacuum and flushed with nitrogen five times. Thereafter, anhydrous DMF (30.0 mL) was added to the flask via cannula transfer. The reaction mixture was then brought to reflux. The flask was cooled to room temperature after 36 hours, after which, 75.0 mL of water was added. The resulting yellow solid mixture was filtered and washed with water. The solid was then transferred into a 250 mL round bottom flask and suspended in 100.0 mL of water. Ethylenediamine (4.0 mL, 59.83 mmol) was added and the suspension was stirred for 1.5 hours at room temperature. The solution was then filtered and the solid was washed with water. The remaining yellow solid was dissolved in acetonitrile and dried with anhydrous $MgSO_4$. The dried solution was then filtered and the acetonitrile was removed under vacuum and heating. The resulting yellow brown residue was recrystallized in dichloromethane and methanol. (0.491 g, 74%). The separation of *E*- and *Z*-isomers was achieved using a silica column and an 8:3 Dichloromethane:Hexanes solvent mixture.

(Z)-4,4'-(1,2-diphenylethene-1,2-diyl)dibenzonitrile (***Z*-1**): ^{13}C NMR (101 MHz, CD_2Cl_2) δ 148.08, 142.33, 141.79, 132.20, 132.14, 131.97, 131.50, 131.43, 128.65,128.43, 127.94, 127.77, 119.02, 111.04 ^{1}H NMR (400 MHz, CD_2Cl_2) δ 7.43 (d, J = 8 , 4H), 7.16-7.11 (m, 10H), 7.02-6.99 (m, 4H). FTIR KBr *v* (cm^{-1}) 2930, 2853, 2231, 1747, 1603, 1372, 1247, 1226

(E)-4,4'-(1,2-diphenylethene-1,2-diyl)dibenzonitrile (***E*-1**): ^{13}C NMR (101 MHz, CD_2Cl_2) δ 148.25, 142.11, 141.83, 132.14, 131.98, 131.51, 128.66, 127.94, 119.94, 110.80 ^{1}H NMR

(400 MHz, CD_2Cl_2) δ 7.41 (d, J = 8, 4H), 7.18-7.12 (m, 10H), 6.99-6.97 (m, 4H) IR KBr *v* (cm^{-1}) 2930, 2853, 2227, 1745, 1605, 1370, 1246, 1224

UV-vis and Photoluminescence. Spectra were taken over a scan range of 250- 450 nm using 0.2 M solutions of ***Z*-1** and ***E*-1** in dichloromethane (Figure 2).

Photoluminescent spectra were taken by first making 20 µM solutions of compound ***Z*-1** and ***E*-1** in THF with varying percentages of water (0%, 10%, 20%, 30%, 40%, 50%, 60%, 70%, 80%, 90% and 95%). Spectra were taken of each solution using an excitation wavelength of 350 nm over the range of 400 – 650 nm. Solid phototluminescence experiements were conducted using a small amount of the compounds ***Z*-1** and ***E*-1** adhered to an aluminium sample stage. Solid spectra were obtained using the same instrument setup as the solution experiments.

Sensing Experiments

Picric Acid (PA) sensing experiments were performed on 95/5 (water/THF) solutions of both ***Z*-1** and ***E*-1** at a concentration of 20 µM. A 0.01 M solution of PA in THF was incrementally added to 1 mL of the of both ***Z*-1** and ***E*-1** solutions. Spectra were taken, using an excitation wavelength of 350 nm, at increasing volumes of added PA solution (0, 1, 2, 3, 4, 5, 6, 7, 8, 9, 10, 11, 12, 13, 14, 15, 16, and 17µL).

Sensing studies were conducted following a modified version of the procedure above for 0.1 M solutions of toluene, nitrobenzene, 4-nitrotoluene, and 2,4-dinitrotoluene (page S21of ESI). Spectra were taken at addition increments of 0, 2.5, 5, 7.5, 10, 12.5, 15, 17.5, 20, 22.5, 25 µL (Figures S25-S28). Plots of I_0/I vs Concentration were generated for all sensing studies. Plots were fit using nonlinear curve fitting and the equation $y = y_0 + Ae^{R_0 x}$. From the fittings, static quenching constants, K_s, were determined for each isomer and substrate combination using the equation $K_s = AR_0$. Where A and R_0 are values determined from the fitting.

Crystallographic Analysis. Colorless crystals of ***E*-1** and pale-yellow crystals of ***Z*-1** suitable for X-ray diffraction analyses were obtained by slow evaporation of solvent from a dichloromethane/methanol solution mixture at room temperature. X-ray intensity data were measured using a Bruker APEX II CCD-based diffractometer with Mo K_α radiation (λ =0.71073 Å). The raw data frames were integrated with the SAINT+ program integrated in APEX 2 interface by using a narrow-frame integration algorithm. Corrections for Lorentz and polarization effects were also applied. Empirical absorption corrections based on the multiple measurements of equivalent reflections were applied by using the program SADABS. All structures were solved with SHELXT.[35-36] Difference Fourier calculations and full-matrix least-squares on F^2 were performed with SHELXL-2016[35-36] using OLEX2.[37] Crystal data, data collection parameters, and results of the analyses are available in the Supporting Information; see Table S1.

Computational Analysis. Geometry optimization calculations were performed with Gaussian 98w,[38] using the B3LYP[39-40] functional and the 6-31G(d) basis set. DFT calculations were performed on both isomers, an un-substituted TPE molecule, and the dimers of ***E*-1** and ***Z*-1**. The molecular orbitals for all molecules and their energies were determined by geometry-optimized calculations that were initiated with the structures as determined from the crystal structure analyses. The calculation of dimers for both ***Z*-1** and ***E*-1** was conducted starting from the two adjacent molecules in the unit cell obtained from the crystal structure. The molecular orbitals of all dimers and their energies were determined by geometry optimization calculations.

RESULTS AND DISCUSSION

Two TPE based *E*/*Z* isomers were obtained from the reaction of $TPEBr_2$ with CuCN in DMF under reflux. Both products were characterized by a combination of FTIR, NMR, MS, and single crystal X-ray diffraction analyses. Both isomers crystallized in the monoclinic crystal system. ORTEP diagrams of the molecular structures of

both isomers are shown in **Figure 1**. Crystallographic data of both compounds are listed in Table S1 in the ESI.

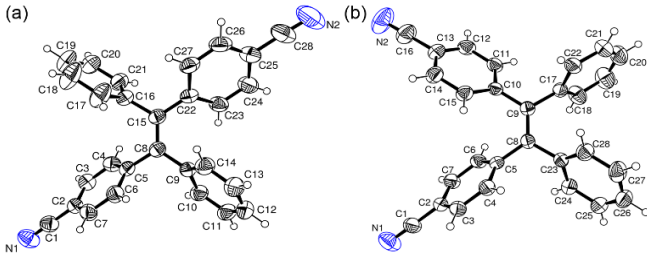

Figure 1. ORTEP diagrams of molecular structures of the two isomers, ***E*-1** (a) and ***Z*-1** (b), showing thermal ellipsoids at the 30% level.

UV-vis absorption spectra were taken for both isomers in dichloromethane solutions. As shown in **Figure 2(a)**, both ***E*-1** and ***Z*-1** have a major absorption band around 330 nm. The only dissimilarity between the two isomers is the absorption intensity between 275 nm and 315 nm. The absorption intensity of ***Z*-1** is slightly higher than that of ***E*-1**. In order to understand the differences between ***Z*-1 and *E*-1**, DFT calculations were conducted. The TDDFT calculated spectra, as shown in **Figure 2(b)**, are in good agreement with the experimental results. The absorption intensity variation is mainly attributed to the excitation from HOMO to LUMO+1. The oscillator strength of this transition is 0.1919 for ***Z*-1** and only 0.0005 for that of ***E*-1**. This is because in ***E*-1,** the HOMO to LUMO+1 transition is forbidden due to its center of inversion symmetry.[41] The larger oscillator strength of ***Z*-1** resulted in stronger absorption.

Since ***E*-1** and ***Z*-1** are TPE derivatives, the PL properties of these isomers were naturally investigated. As shown in **Figure 3**, unlike the non-emissive behavior of TPE, the THF solutions of both isomers are still emissive. Interestingly, the emission spectra of both ***E*-1** and ***Z*-1** in THF solutions show three major emission peaks, two peaks located at 408 nm and 433 nm, and one shoulder at 458 nm. Unexpectedly, when varying amounts of water were added to the THF solutions of ***E*-1** and ***Z*-1**, the emission intensity was not enhanced with increasing water

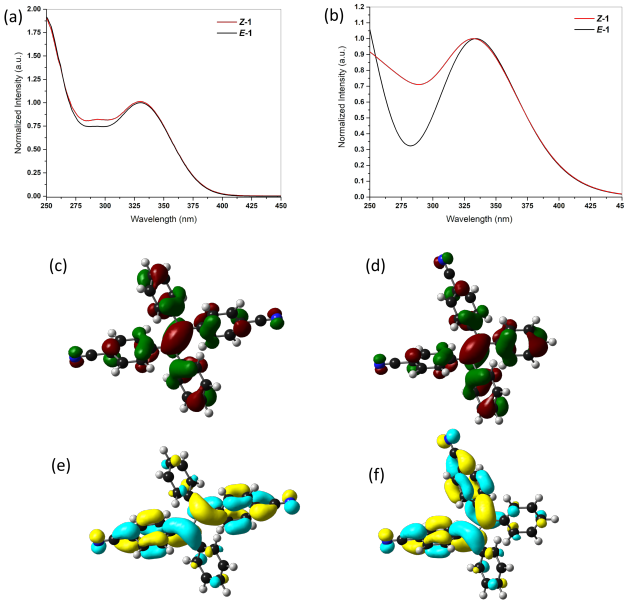

Figure 2: Experimental UV-Vis absorption spectra of ***Z*-1** and ***E*-1** in dichloromethane, (a), TDDFT calculated UV-Vis absorption spectra of ***Z*-1** and ***E*-1** (b). Molecular orbitals of ***E*-1**and ***Z*-1**. HOMO (c) -6.0012 eV and LUMO (e) -2.2183 eV of ***E*-1**. HOMO (d) -5.9868 eV and LUMO -2.2079 eV (f) of ***Z*-1.**

fractions. As illustrated in **Figure 3**, for ***Z*-1**, when water fractions (f_w) were 10% and 20%, enhanced emission intensities were observed, however, the intensity dropped dramatically when f_w = 30%. When 40% of water was added to the THF solution of ***Z*-1**, the PL intensity increased again, the PL intensities of solutions with f_w = 50%, and 60% were very weak. Intriguingly, when f_w = 70%, the major emission peak red-shifted to 486 nm along with a weak peak around 400 nm. As the water fraction was increased to 80%, the intensity of the peak at 486 nm increased. The solutions with f_w = 90% and f_w = 95% show dramatic intensity enhancement by more than 10-fold. Images of the solutions containing different water contents were taken under 365 nm UV light in the dark, as shown in lower **Figure 3(a)**. The vials with 10% and 20% water emit a bright blue color, and the solutions containing 90% and 95% water emit a bright cyan color. The relative brightness of these emissions matches very well with the fluorescent intensity in the spectra. The emission colors of these solutions were plotted as a CIE color diagram as shown in **Figure 3(b)**.

Interestingly, the emission color gradually shifted from deep-blue to lighter blue when $f_w \leq 60\%$. When $f_w \geq 70\%$, the emission color shifted to the turquoise region and when the water content was 90% or 95% the color further shifted to the green-blue region. The colors from the CIE diagram matched very well with that observed from the emission spectra and the solutions under UV light. Similar phenomena were observed for the ***E*** isomer as illustrated in **Figure 3(c)** and **(d)**.

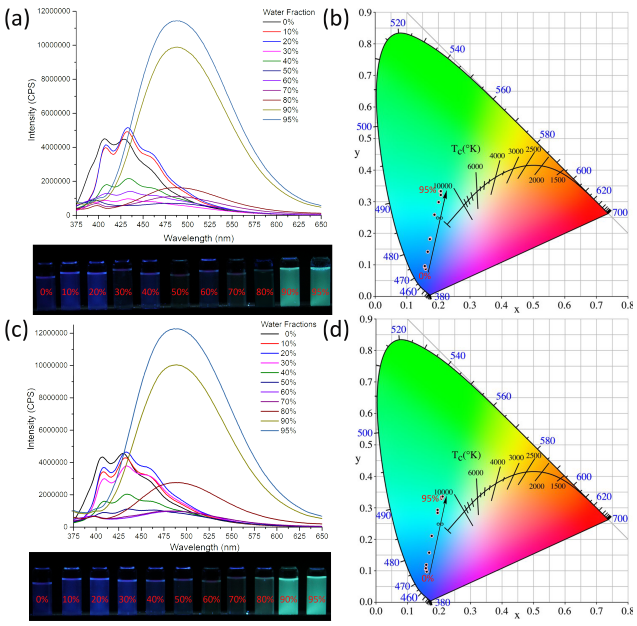

Figure 3. Emission spectra (top) and image under 365 nm UV light (bottom) for solutions of ***Z*-1** in water-THF solutions with varying water fractions, (a). CIE color diagram for the emission of ***Z*-1** with different water fractions, (b). PL spectra (top) and image under 365 nm UV light (bottom) for solutions of ***E*-1** with varying water fractions, (c). CIE color diagram for the emission of ***E*-1** with different water fractions, (d).

As discussed above, both the ***E*-1** and ***Z*-1** isomers possess aggregation induced emission red-shift (AIERS) behavior, which stands apart from that of non-substituted TPE. According to the literature, the emission red-shift originates from the formation of excimers. The intermolecular interaction not only restricted the intramolecular rotation of the phenyl rings, but also played an important role in the electron transition process within and between molecules.[42] To the best of our knowledge, only a few AIERS examples for small molecules and quantum dots have been reported.[43] A recent report, by Li and coworkers, studied the mechanoluminescence of a tetra-substituted TPE molecule, where emission red-shift was observed.[44] Many examples of aggregation-induced emission blue-shift for small molecules and coordination polymers have been studied.[17-18, 26, 45]

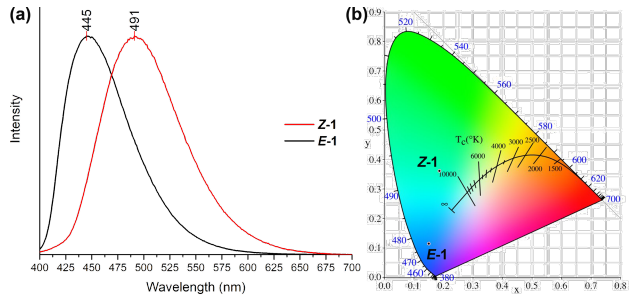

Figure 4. (a) solid state PL spectra of ***E*-1** and ***Z*-1**. (b) The CIE color space chromaticity diagram showing the emission color of ***E*-1** and ***Z*-1.**

Though the photoluminescence of ***E*-1** and ***Z*-1** are very similar in solution, surprisingly, the crystalline solids show distinct emission maxima. As illustrated in **Figure 4** (a), the emission curve of the trans-isomer, ***E*-1**, has a maximum at 445 nm, while the cis-isomer, ***Z*-1**, shifted to 491 nm upon excitation at the same wavelength. The emission colors of both isomers are shown in the CIE diagram in **Figure 4 (b)**. We hypothesize that the differences between ***E*-1** and ***Z*-1** originate from the different molecular packing. Though both isomers crystallized in monoclinic crystal system, the unit cell parameters are different.

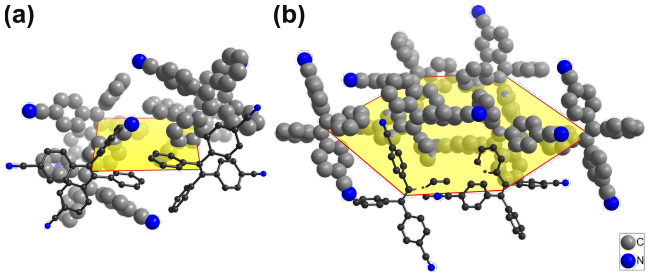

Figure 5. Molecular packing of ***Z*-1** (a) and ***E*-1** (b) within one unit cell.

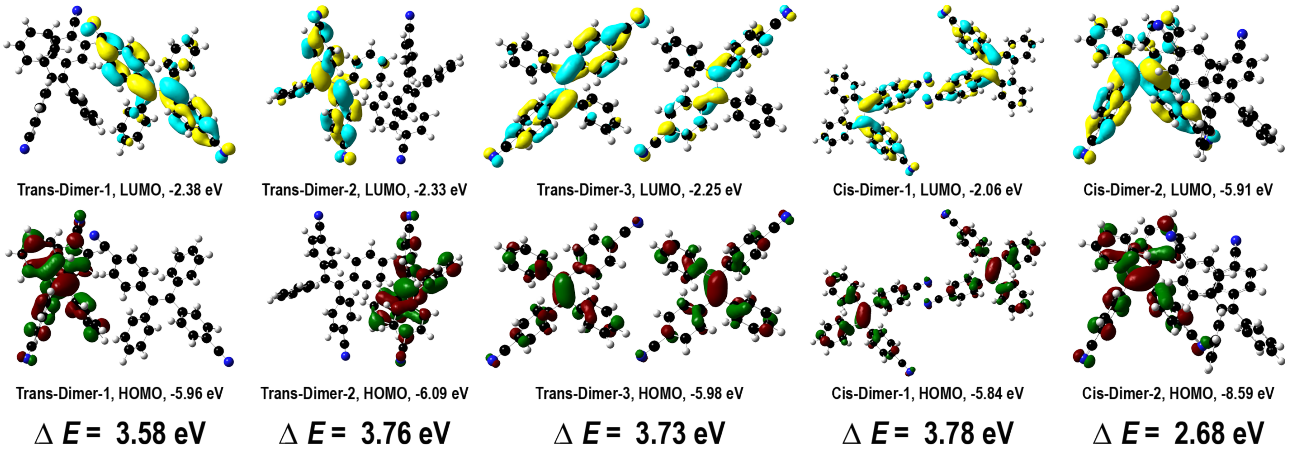

Figure 6. Frontier molecular orbitals and energy gaps between HOMO and LUMO of dimers of the ***cis*** (***Z*-1**) and ***trans*** ***(E-1)*** isomers.

There are 8 molecules in the unit cell of ***E*-1** and two molecules in the asymmetric unit, while the unit cell of ***Z*-1** contains 4 molecules, with only one molecule in the asymmetric unit. As shown in **Figure 5**, the centers of these molecules are in a plane. The smallest distance between two molecules for ***Z*-1** is 5.910 Å, while this distance is 7.099 Å for that of ***E*-1**. The variable distances between molecules resulted in differences in molecular configurations. It is likely that the molecules in the ***Z*-1** crystal can form excimers.

To understand the nature of the two isomers, DFT calculations were conducted. As expected, the geometry optimization calculations resulted in two isomers with almost identical HOMO and LUMO energy levels. This is in good agreement with the solution phase UV-Vis absorption spectra and photoluminescence. Compunds ***E*-1** and ***Z*-1** were also compared with un-substituted TPE. Though the HOMOs of all three compounds look similar, the energies are slightly different, -6.00 eV and – 5.98 eV for the HOMOs of ***E*-1** and ***Z*-1**, respectively, but – 5.32 eV for that of TPE. The energies of the LUMOs are – 2.22 eV, - 2.21 eV, and – 1.20 eV for ***E*-1**, ***Z*-1,** and TPE, respectively. The HOMO – LUMO gap for the TPE molecule is 4.11 eV which is slightly larger than that of 3.78 eV for both ***E*-1** and ***Z*-1**. (ESI)

To help us gain further insights into the electronic structures and molecular orbitals (MOs) of the isomers in the solid state, dimers from both crystal structures were selected and geometry optimization calculations were conducted. As shown in **Figure 6**, three dimers in ***E*-1** and two dimers in ***Z*-1** were selected. The HOMOs of the dimers for the trans (***E*-1**) isomer possess energies between -5.96 eV to -6.09 eV, and LUMOs with energies between -2.25 ev to -2.38 eV. The HOMO-LUMO energy gaps are -3.58 eV, -3.76 eV, and -3.73 eV for dimers 1, 2, and 3, respectively, with an average energy gap of- 3.69 eV. In Trans-Dimer-1 and Trans-Dimer-2, the HOMO is located on one molecule but the LUMO is located on another. However, for Trans-Dimer-3, HOMO and LUMO are located on both monomers.

For the ***Z-1*** isomer, there are two dimers possible, as shown in **Figure 6**. Cis-Dimer-1 possesses a HOMO at -5.84 eV and LUMO at -2.06 eV with an energy gap of 3.78 eV, which is very similar to that of the *trans*-dimers. For the second cis-dimer, however, the energies of the HOMO and LUMO are very different. Cis-Dimer-2 of the *cis* isomer contains a HOMO at -8.59 eV and a LUMO at -5.91 eV, with an energy gap of 2.68 eV. This is much smaller than that of all the *trans* dimers. This indicates that the Cis-Dimer-2 can be considered an excimer. The formation of an excimer would cause the emission of the *cis* isomer to be red-shifted, which was observed as shown in **Figure 4 (a)**. Another representative property of excimers is that they usually possess

longer luminescent lifetimes. Bearing this in mind, crystals of both isomers were used for the lifetime measurements. The lifetime of the *trans* isomer was measured to be 2.333 ± 0.004 ns while the *cis*-isomer's lifetime was determined to be 3.895 ± 0.004 ns. The luminescent lifetime of the *cis* isomer is almost double the lifetime of the *trans* isomer, in very good agreement with the DFT calculations.

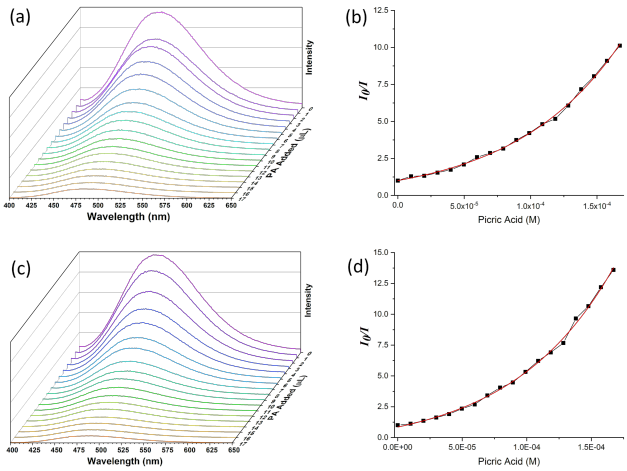

Figure 7. PL spectra of ***Z*-1**, (a), and ***E*-1**, (c), in THF/water mixtures (f_w=95%) with different amounts of Picric Acid (PA). (b) Plot of I_0/I vs PA concentration in ***Z*-1**, (b), and ***E*-1**, (d), solutions (f_w=95).

AIE type materials have been shown to act as chemosensors for the detection of nitroaromatic explosives.[30] Picric acid was first selected as the substrate because it is very similar to TNT. Picric acid sensing experiments of both ***Z*-1** and ***E*-1** at f_w=95% were conducted. The PL intensities of both ***Z*-1** and ***E*-1** are weakened with the addition of picric acid. As illustrated in **Figure 7 (a) and (c)**, the PL intensity for both isomers dropped sequentially when increasing amounts of picric acid solution was added. The Stern–Volmer plot of the inverse relative PL intensity (I_0/I) versus picric acid concentration for ***Z*-1** and ***E*-1** are given in **Figure 5(b)** and **(d)** respectively, which yielded upward curving plots. Similar plots have been reported for conjugated polymers.[29]

To evaluate the sensing selectivity of ***E*-1** and ***Z*-1** torward different nitroaromatics, nitrobenzene, nitrotoluene and dinitrotoluene sensing experiments were also conducted. Toluene sensing was also performed as a blank experiment. As can be seen in **Figure 8**, when ***E*-1** was used, the $(I_0-I)/I$ quenching effiency for picric acid is 43, while all other substrates are below 0.3. When ***Z*-1** was used, the $(I_0-I)/I$ value for picric acid is 21, while all other substrates are below 0.2. This result indicates that both ***E*-1** and ***Z*-1** can selectively detect picric acid over other nitroaromatics, with ***E*-1** having a higher sensitivity than ***Z*-1**. The static quenching constant for picric acid is 22,362 L mol^{-1} for ***E*-1**, and 16,281 L mol^{-1} for ***Z*-1.** The static quenching constant for other aromatics are all below 800 L mol^{-1} for both isomers. Interestingly, the static quenching constants of nitrotoluene, dinitrotoluene, and nitrobenzene are very similar to that of toluene, indicating that neither isomer can distinguish these nitroaromatics when the concentration is too low. Both isomers are excellent sensers in the detection of picric acid at concentrations lower than 10 µM.

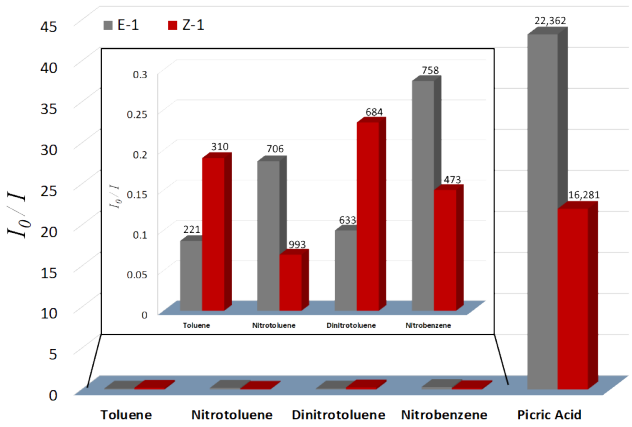

Figure 8: Histogram of $(I_0-I)/I$ for both E-1 and Z-1. Where I_0 and I equal the max intensity of PL spectra at 0 M and 2.44 x 10^{-3} M quenching substrate, respectively. Numbers above bars represent the static quenching constant, K_s.

It is well-known that the nitroaromatics quench luminescence due to the photoinduced electron-transfer (PET) process, in which, the nitroaromatics accept the excited electrons from the fluorophore, and the energy will be released through non-radiative decay pathways.[46] For the PET process to take place the energy level(s) of

the unoccupied molecular orbital(s) of nitroaromatics must be lower than that of the fluorophore to allow elelctrons to flow from fluorophore to the empty orbitals of nitroaomatic molecues. To gain deep insights about the selective sensing of ***E*-1** and ***Z*-1**, geometry optimization DFT calculations were conducted on different nitroaromatic compounds to compare with that of ***E*-1**. As shown in **Figure 9**, the HOMO of ***E*-1** has an energy of -6.00 eV and it is -2.22 eV for that of LUMO. The calculation indicated that the LUMO of nitrobenzene sits at -2.43 eV, which is below the LUMO of ***E*-1**. The LUMO+1 for nitrobenzene, however, is much high in energy (-0.755 eV) than the LUMO of ***E*-1**. Similar results were obtained for Nitrotoluene, in which the LUMO and LUMO +1 have energies of -2.32 eV and -0.681 eV, respectively. Remarkablly, there are three LUMOs (LUMO, LUMO+1, LUMO+2) in PA that lie inbetween the HOMO and LUMO of ***E*-1**. Therefore, it is much easier for excited electrons in ***E*-1** to transfor to PA as there are three available LUMOs, which explains the high quenching efficeincy of PA over other nitroaromatics. Another aspect that has to be taken into consideration is that PA is much more soluble in water than other nitroaromatics, and we used f_w=95% suspension for the quenching tests. Since trinitrotoluene, TNT, is not safe to handle, we conducted the DFT calculation to reveal the unoccupied MOs of TNT. Suprisingly, the MOs of TNT are very similar to that of PA. The energies of LUMO, LUMO+1 and LUMO+2 are all lower than that of LUMO of ***E*-1**. This indicated that ***E*-1** should be very sensitive in TNT detection as well.

CONCLUSION

In conclusion, we have demonstrated experimentally and theoretically that the dicyanido substituted TPE molecules exhibit distinct emission red-shift behavior. The distinct emission differences in the solid state between ***E*-1** and ***Z*-1** originated from the formation of excimers due to the different packing of molecules in the solid state. Explosive sensing experiments demonstrated that both ***E*-1** and ***Z*-1** isomers are very good chemosensors for the detection of picric acid at very low concentrations. DFT calculation indicated that the PET process is more favorable in PA as there are three LUMOs that can accept electrons from the excited states of ***E*-1**.

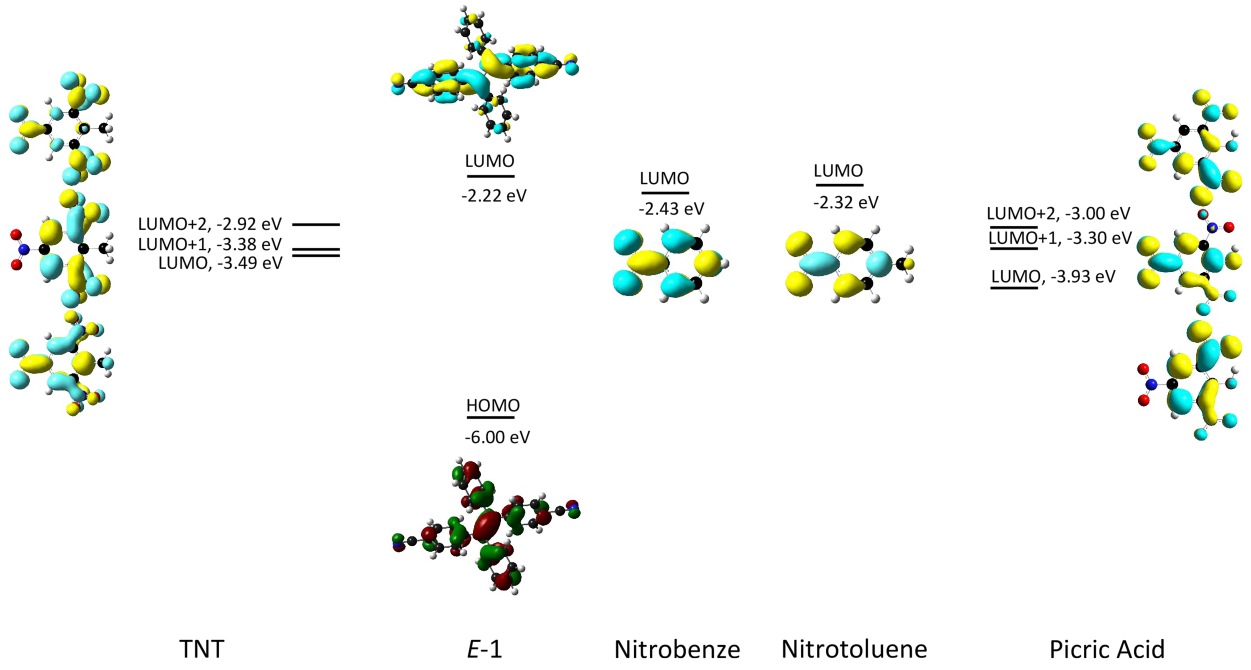

Figure 9: Representative MOs and energy levels of ***E*-1** and LUMOs of nitroaromatic compounds that are lower than the LUMO of ***E*-1**.

ASSOCIATED CONTENT

Supporting Information

Experimental details, including synthesis, characterization, additional spectra, additional images and X-ray crystallographic data of compounds *Z*-1 and *E*-1. This information is available free of charge via the Internet at https://pubs.acs.org.

Crystallographic Data

CCDC 1570894-1570895 contain the supplementary crystallographic data of ***Z*-1** and ***E*-1**. These data can be obtained free of charge via www.ccdc.cam.ac.uk/data_request/cif, or by emailing data_request@ccdc.cam.ac.uk.

AUTHOR INFORMATION

Corresponding Author

*Email: q.zhang@wsu.edu

Notes

The authors declare no competing financial interest.

ACKNOWLEDGMENT

This work is supported by the Washington State University startup funds. We thank Jesse Huso and Dr. Matthew D. McCluskey for the use of their fluorimeter and help with lifetime measurements. MJH would also like to thank the Frank A. Fowler Endowed Graduate Fellowship in Chemistry at Washington State University for financial support. The Bruker (Siemens) SMART APEX diffraction facility was established at the University of Idaho with the assistance of the NSF-EPSCoR program and the M. J. Murdock Charitable Trust, Vancouver, WA.

ABBREVIATIONS

AIE, AIEE, RIR, ACQ, HOMO, LUMO, OLED, DFT, TPE, PA, TNT, PET

REFERENCES

1. Hu, Z.; Deibert, B. J.; Li, J., Luminescent metal-organic frameworks for chemical sensing and explosive detection. *Chem. Soc. Rev.* **2014,** *43* (16), 5815-5840.

2. Chen, X.; Wang, F.; Hyun, J. Y.; Wei, T.; Qiang, J.; Ren, X.; Shin, I.; Yoon, J., Recent progress in the development of fluorescent, luminescent and colorimetric probes for detection of reactive oxygen and nitrogen species. *Chem. Soc. Rev.* **2016,** *45* (10), 2976-3016.

3. Cui, Y.; Zhu, F.; Chen, B.; Qian, G., Metal-organic frameworks for luminescence thermometry. *Chem. Commun.* **2015,** *51* (35), 7420-7431.

4. Sun, C.-Y.; Wang, X.-L.; Zhang, X.; Qin, C.; Li, P.; Su, Z.-M.; Zhu, D.-X.; Shan, G.-G.; Shao, K.-Z.; Wu, H.; Li, J., Efficient and tunable white-light emission of metal–organic frameworks by iridium-complex encapsulation. *Nat. Commun.* **2013,** *4*, 2717.

5. Lan, A.; Li, K.; Wu, H.; Olson, D. H.; Emge, T. J.; Ki, W.; Hong, M.; Li, J., A Luminescent Microporous Metal–Organic Framework for the Fast and Reversible Detection of High Explosives. *Angew. Chem. Int. Ed.* **2009,** *48* (13), 2334-2338.

6. Banerjee, D.; Hu, Z.; Pramanik, S.; Zhang, X.; Wang, H.; Li, J., Vapor phase detection of nitroaromatic and nitroaliphatic explosives by fluorescence active metal-organic frameworks. *CrystEngComm* **2013,** *15* (45), 9745-9750.

7. Hu, Z.; Huang, G.; Lustig, W. P.; Wang, F.; Wang, H.; Teat, S. J.; Banerjee, D.; Zhang, D.; Li, J., Achieving exceptionally high luminescence quantum efficiency by immobilizing an AIE molecular chromophore into a metal-organic framework. *Chem. Commun.* **2015,** *51* (15), 3045-3048.

8. Lustig, W. P.; Mukherjee, S.; Rudd, N. D.; Desai, A. V.; Li, J.; Ghosh, S. K., Metal-organic frameworks: functional luminescent and photonic materials for sensing applications. *Chem. Soc. Rev.* **2017,** *46* (11), 3242-3285.

9. Hong, Y.; Lam, J. W. Y.; Tang, B. Z., Aggregation-induced emission. *Chem. Soc. Rev.* **2011,** *40* (11), 5361-5388.

10. Fang, C.; Xie, Y.; Johnston, M. R.; Ruan, Y.; Tang, B. Z.; Peng, Q.; Tang, Y., SERS and NMR Studies of Typical Aggregation-Induced Emission Molecules. *J. Phys. Chem. A* **2015,** *119* (29), 8049-8054.

11. Zhao, Z.; Tang, B. Z., Tetraarylethenes and Aggregation-Induced Emission. In *Polycyclic Arenes and Heteroarenes*, Wiley-VCH Verlag GmbH & Co. KGaA: 2015; 193-222.

12. Mei, J.; Leung, N. L. C.; Kwok, R. T. K.; Lam, J. W. Y.; Tang, B. Z., Aggregation-Induced Emission: Together

We Shine, United We Soar! *Chem. Rev.* **2015,** *115* (21), 11718-11940.
13. Wu, W.; Tang, R.; Li, Q.; Li, Z., Functional hyperbranched polymers with advanced optical, electrical and magnetic properties. *Chem. Soc. Rev.* **2015,** *44* (12), 3997-4022.
14. Zhao, Z.; Lam, J. W. Y.; Tang, B. Z., Tetraphenylethene: a versatile AIE building block for the construction of efficient luminescent materials for organic light-emitting diodes. *J. Mater. Chem.* **2012,** *22* (45), 23726-23740.
15. Shi, J.; Deng, Q.; Wan, C.; Zheng, M.; Huang, F.; Tang, B., Fluorometric probing of the lipase level as acute pancreatitis biomarkers based on interfacially controlled aggregation-induced emission (AIE). *Chem. Sci.* **2017,** *8* (9), 6188-6195.
16. Dong, J.; Zhang, K.; Li, X.; Qian, Y.; Zhu, H.; Yuan, D.; Xu, Q.-H.; Jiang, J.; Zhao, D., Ultrathin two-dimensional porous organic nanosheets with molecular rotors for chemical sensing. *Nat. Commun.* **2017,** *8* (1), 1142.
17. Shustova, N. B.; McCarthy, B. D.; Dincă, M., Turn-On Fluorescence in Tetraphenylethylene-Based Metal–Organic Frameworks: An Alternative to Aggregation-Induced Emission. *J. Am. Chem. Soc.* **2011,** *133* (50), 20126-20129.
18. Zhang, Q.; Su, J.; Feng, D.; Wei, Z.; Zou, X.; Zhou, H.-C., Piezofluorochromic Metal–Organic Framework: A Microscissor Lift. *J. Am. Chem. Soc.* **2015,** *137* (32), 10064-10067.
19. Allendorf, M. D.; Bauer, C. A.; Bhakta, R. K.; Houk, R. J. T., Luminescent metal-organic frameworks. *Chem. Soc. Rev.* **2009,** *38* (5), 1330-1352.
20. Gong, Q.; Hu, Z.; Deibert, B. J.; Emge, T. J.; Teat, S. J.; Banerjee, D.; Mussman, B.; Rudd, N. D.; Li, J., Solution Processable MOF Yellow Phosphor with Exceptionally High Quantum Efficiency. *J. Am. Chem. Soc.* **2014,** *136* (48), 16724-16727.
21. Lustig, W. P.; Wang, F.; Teat, S. J.; Hu, Z.; Gong, Q.; Li, J., Chromophore-Based Luminescent Metal–Organic Frameworks as Lighting Phosphors. *Inorg. Chem.* **2016,** *55* (15), 7250-7256.
22. Deibert, B. J.; Velasco, E.; Liu, W.; Teat, S. J.; Lustig, W. P.; Li, J., High-Performance Blue-Excitable Yellow Phosphor Obtained from an Activated Solvochromic Bismuth-Fluorophore Metal–Organic Framework. *Cryst. Growth Des.* **2016,** *16* (8), 4178-4182.
23. Wang, F.; Liu, W.; Teat, S. J.; Xu, F.; Wang, H.; Wang, X.; An, L.; Li, J., Chromophore-immobilized luminescent metal-organic frameworks as potential lighting phosphors and chemical sensors. *Chem. Commun.* **2016,** *52* (67), 10249-10252.
24. Zhang, M.; Feng, G.; Song, Z.; Zhou, Y.-P.; Chao, H.-Y.; Yuan, D.; Tan, T. T. Y.; Guo, Z.; Hu, Z.; Tang, B. Z.; Liu, B.; Zhao, D., Two-Dimensional Metal–Organic Framework with Wide Channels and Responsive Turn-On Fluorescence for the Chemical Sensing of Volatile Organic Compounds. *J. Am. Chem. Soc.* **2014,** *136* (20), 7241-7244.
25. Wang, H.; Bao, Z.; Wu, H.; Lin, R. B.; Zhou, W.; Hu, T. L.; Li, B.; Zhao, J. C.; Chen, B., Two solvent-induced porous hydrogen-bonded organic frameworks: solvent effects on structures and functionalities. *Chem. Commun.* **2017,** *53* (81), 11150-11153.
26. Wei, Z.; Gu, Z.-Y.; Arvapally, R. K.; Chen, Y.-P.; McDougald, R. N.; Ivy, J. F.; Yakovenko, A. A.; Feng, D.; Omary, M. A.; Zhou, H.-C., Rigidifying Fluorescent Linkers by Metal–Organic Framework Formation for Fluorescence Blue Shift and Quantum Yield Enhancement. *J. Am. Chem. Soc.* **2014,** *136* (23), 8269-8276.
27. Bhunia, A.; Vasylyeva, V.; Janiak, C., From a supramolecular tetranitrile to a porous covalent triazine-based framework with high gas uptake capacities. *Chem. Commun.* **2013,** *49* (38), 3961-3963.
28. Wang, X.; Zhang, C.; Zhao, Y.; Ren, S.; Jiang, J.-X., Synthetic Control and Multifunctional Properties of Fluorescent Covalent Triazine-Based Frameworks. *Macromol. Rapid Commun.* **2016,** *37* (4), 323-329.
29. Journal of Materials Chemistry BDalton TransactionsHu, R.; Lam, J. W. Y.; Liu, J.; Sung, H. H. Y.; Williams, I. D.; Yue, Z.; Wong, K. S.; Yuen, M. M. F.; Tang, B. Z., Hyperbranched conjugated poly(tetraphenylethene): synthesis, aggregation-induced emission, fluorescent photopatterning, optical limiting and explosive detection. *Polym. Chem.* **2012,** *3* (6), 1481-1489.
30. Qin, A.; Lam, J. W. Y.; Tang, B. Z., Luminogenic polymers with aggregation-induced emission characteristics. *Prog. Polym. Sci.* **2012,** *37* (1), 182-209.
31. Yang, Z.; Qin, W.; Leung, N. L. C.; Arseneault, M.; Lam, J. W. Y.; Liang, G.; Sung, H. H. Y.; Williams, I. D.; Tang, B. Z., A mechanistic study of AIE processes of TPE luminogens: intramolecular rotation vs. configurational isomerization. *J. Mater. Chem. C* **2016,** *4* (1), 99-107.
32. Tseng, N.-W.; Liu, J.; Ng, J. C. Y.; Lam, J. W. Y.; Sung, H. H. Y.; Williams, I. D.; Tang, B. Z., Deciphering mechanism of aggregation-induced emission (AIE): Is

E-Zisomerisation involved in an AIE process? *Chem. Sci.* **2012,** *3* (2), 493-497.
33. Liang, J.; Shi, H.; Kwok, R. T. K.; Gao, M.; Yuan, Y.; Zhang, W.; Tang, B. Z.; Liu, B., Distinct optical and kinetic responses from E/Z isomers of caspase probes with aggregation-induced emission characteristics. *J. Mater. Chem. B* **2014,** *2* (27), 4363-4370.
34. Zhao, E.; Li, H.; Ling, J.; Wu, H.; Wang, J.; Zhang, S.; Lam, J. W. Y.; Sun, J. Z.; Qin, A.; Tang, B. Z., Structure-dependent emission of polytriazoles. *Polym. Chem.* **2014,** *5* (7), 2301-2308.
35. Sheldrick, G., SHELXT - Integrated space-group and crystal-structure determination. *Acta Crystallogr. Sect. A: Found. Crystallogr.* **2015,** *71* (1), 3-8.
36. Sheldrick, G., A short history of SHELX. *Acta Crystallogr. Sect. A: Found. Crystallogr.* **2008,** *64* (1), 112-122.
37. Dolomanov, O. V.; Bourhis, L. J.; Gildea, R. J.; Howard, J. A. K.; Puschmann, H., OLEX2: a complete structure solution, refinement and analysis program. *J. Appl. Crystallogr.* **2009,** *42* (2), 339-341.
38. Gaussian 98 (Revision A.7), M. J. F., G. W. Trucks, H. B. Schlegel, G. E. Scuseria, M. A. Robb, J. R. Cheeseman, V. G. Zakrzewski, J. A. Montgomery, R. E. Stratmann, J. C. Burant, S. Dapprich, J. M. Millam, A. D. Daniels, K. N. Kudin, M. C. Strain, O. Farkas, J. Tomasi, V. Barone, M. Cossi, R. Cammi, B. Mennucci, C. Pomelli, C. Adamo, S. Clifford, J. Ochterski, G. A. Petersson, P. Y. Ayala, Q. Cui, K. Morokuma, D. K. Malick, A. D. Rabuck, K. Raghavachari, J. B. Foresman, J. Cioslowski, J. V. Ortiz, B. B. Stefanov, G. Liu, A. Liashenko, P. Piskorz, I. Komaromi, R. Gomperts, R. L. Martin, D. J. Fox, , T. Keith, M. A. Al-Laham, C. Y. Peng, A. Nanayakkara, C. Gonzalez, M. Challacombe, P. M. W. Gill, B. G. Johnson, W. Chen, M. W. Wong, J. L. Andres, M. Head-Gordon, E. S. Replogle, and J. A. Pople, Gaussian, Inc., *Gaussian 98*, Pittsburgh, PA, , 1998.
39. Becke, A. D., Density-functional thermochemistry. III. The role of exact exchange. *J. Chem. Phys.* **1993,** *98*, 5648-5652.
40. Lee, C.; Yang, W.; Parr, R. G., Development of the Colle-Salvetti correlation-energy formula into a functional of the electron density. *Phys. Rev. B: Condens. Matter* **1988,** *37* (2), 785-789.
41. Laporte, O.; Meggers, W. F., Some Rules of Spectral Structure*. *J. Opt. Soc. Am.* **1925,** *11* (5), 459-463.
42. Li, Q.; Li, Z., The Strong Light-Emission Materials in the Aggregated State: What Happens from a Single Molecule to the Collective Group. *Adv. Sci.* **2017,** *4* (7), 1600484.
43. Li, Y.; Lin, H.; Luo, C.; Wang, Y.; Jiang, C.; Qi, R.; Huang, R.; Travas-sejdic, J.; Peng, H., Aggregation induced red shift emission of phosphorus doped carbon dots. *RSC Adv.* **2017,** *7* (51), 32225-32228.
44. Xie, Y.; Tu, J.; Zhang, T.; Wang, J.; Xie, Z.; Chi, Z.; Peng, Q.; Li, Z., Mechanoluminescence from pure hydrocarbon AIEgen. *Chem. Commun.* **2017,** *53* (82), 11330-11333.
45. Yang, X.; Lu, R.; Zhou, H.; Xue, P.; Wang, F.; Chen, P.; Zhao, Y., Aggregation-induced blue shift of fluorescence emission due to suppression of TICT in a phenothiazine-based organogel. *J. Colloid Interface Sci.* **2009,** *339* (2), 527-532.
46. Ma, X.; Tao, F.; Zhang, Y.; Li, T.; Raymo, F. M.; Cui, Y., Detection of nitroaromatic explosives by a 3D hyperbranched σ–π conjugated polymer based on a POSS scaffold. *J. Mater. Chem. A* **2017,** *5* (27), 14343-14354.

For Table of Contents Use Only

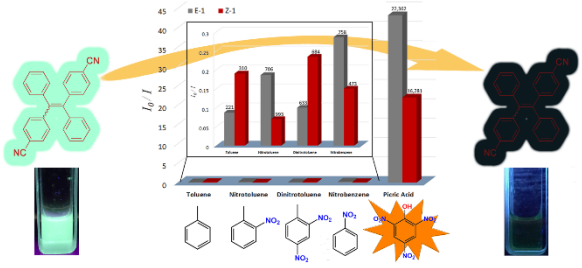

Dicyano substituted TPE isomers prove high selectivity for Picric Acid detection in nitroaromatics sensing.